International Journal of Heat and Mass Transfer 69 (2014) 424–437

Contents lists available at ScienceDirect

International Journal of Heat and Mass Transfer

journal homepage: www.elsevier.com/locate/ijhmt

Nonlinear thermomechanical finite-element modeling, analysis and characterization of multi-turn oscillating heat pipes

Hao Peng, P. Frank Pai *, Hongbin Ma

Department of Mechanical and Aerospace Engineering, University of Missouri, Columbia, MO 65211, USA

ARTICLE INFO

Article history:
Received 26 June 2013
Received in revised form 19 October 2013
Accepted 19 October 2013
Available online 13 November 2013

Keywords:
Oscillating heat pipe
Nonlinear thermomechanical modeling
Finite-element analysis
Modal vibration
Time–frequency analysis
Euler predictor–corrector method

ABSTRACT

Oscillating heat pipes (OHPs) are promising heat dissipation devices for modern electronic systems due to their high heat transfer rate, simple construction and low manufacturing cost. Despite the unique features of OHPs, how to initiate and sustain the slug flow within the capillary tube and how different parameters affect the performance of an OHP are not well understood. This paper presents an advanced, fully nonlinear thermomechanical finite-element model that can simulate the parametrically excited oscillation of the liquid slug, the temperature distribution along the two-phase flow and the heat transfer performance of OHPs. The model can account for the influences of nonlinear spring effect of vapor slugs, interphase mass-transferring effect, fluid filling ratio, operating temperatures of the evaporator and condenser, different heating modes (top- or bottom-heating), gravity, bending pressure loss, properties of the working fluid, and different random distributions of initial velocities and lengths of fluid slugs. An Euler predictor–corrector method with convergence check is used to solve for the oscillation of and the temperature distribution within each fluid plug. The dynamics of OHPs is characterized using a newly developed time–frequency analysis technique. Numerical results show that an OHP is a parametrically excited nonlinear thermomechanical system. Latent heat transfer provides the driving force for the oscillation, and sensible heat transfer induced by forced convection contributes more than 80% of the total heat transfer rate. Generally speaking, working fluids with high thermal conductivity, low latent heat, and low viscosity are favorable for efficient heat transfer. These results provide better understanding of heat transfer mechanisms of OHPs and can be used for design optimization of OHPs.

1. Introduction

With everlasting miniaturization of microelectronic systems and highly developed high-density packaging technology, electronic industry has achieved a prominent development in recent years. Electronics, computers for instance, have decreased from a giant machine to a portable laptop. Although high-density packaging of integrated circuits (ICs) has brought us convenient working environment, powerful computation capability and fast development in space technology, compactly assembled circuits and high-power electronic components also produce large magnitudes of heat fluxes, leaving thermal engineers new challenges of thermal management of these electronic devices. Electronics with a local heat flux from 10 W/cm^2 to 40 W/cm^2 and a total heat power from 10 W to 150 W are already commonly seen in the electronic market [1]. A newly designed high density computer chip for next generation desktops can produce as much as 80 W/cm^2 heat flux with a total heat power of 300 W. Metal oxide semiconductor controlled thyristors can reach a heat flux from 150 W/cm^2 to 200 W/cm^2. Moreover, some laser diode devices can even generate a heat flux of 500 W/cm^2 [2]. If not being effectively dissipated, such large amount of heat will be amassed inside of computer chips, temperature of circuits will increase dramatically, and normal functions of computers will be seriously affected. In addition, the reliability of a silicon chip decreases by 10% for every 2 °C temperature rise and a typical temperature limit for a silicon chip is about 125 °C [3]. According to a survey of the U.S. Air Force, about 55% electronics failures are caused by superheat [3]. If proper thermal management is conducted to control the electronics temperature, electronics can be more durable and reliable.

Traditional heat rejection methods include convective heat transfer devices, heat sinks and etc. The most popular way of dissipating heat out of CPUs is to mount an electric fan on an aluminum heat sink. Heat generated inside a computer chip is conducted to the adjacent heat sink and then dissipated through the large contact area between the metal fins and the flowing air by forced convection. Despite wide applications of these heat dissipation methods in mechanical manufacturing factories, transformer stations and super computers, it is still impossible to dissipate a

* Corresponding author. Address: E2403C Lafferre Hall, Department of Mechanical and Aerospace Engineering, University of Missouri, Columbia, MO 65211, USA. Tel.: +1 (573)884 1474; fax: +1 (573)884 5090.
E-mail address: PaiP@missouri.edu (P.F. Pai).

0017-9310/$ - see front matter © 2013 Elsevier Ltd. All rights reserved.
http://dx.doi.org/10.1016/j.ijheatmasstransfer.2013.10.041

localized heat flux up to 500 W/cm^2 by conventional thermal rejection methods. Applications of heat sinks are limited due to their low thermal conductivity, big sizes and heavy weight associated with metal fins. Additional pumps together with pump power supplies are needed if cooling jets are impinged into a forced-convection system [4]. Hence, effective thermal management is becoming a critical issue to be resolved due to urgent and continuous demand of microelectronic systems.

In order to meet the critical demand in the thermal management field, convention heat pipes (CHPs) were designed in 1960s [5]. CHPs are two-phase capillary-driven passive heat-removal devices in which phase change of the working fluid is the main way of removing heat. A flat hollow metal plate with wick structures inside is an important design of CHPs. Working fluids are partially filled into the space formed among pores. When heat flux is added to one end of a CHP from the bottom of the metal base, the working fluid evaporates and the curvature of the liquid–vapor interface becomes larger and results in the capillary pressure. Driven by the capillary pressure, working fluid is pumped from the condenser section to the evaporator section and meanwhile the vapor is transmitted to the condenser section where the heat is removed [4]. The high transport capability of the capillary flow and the high phase-change heat transfer rate give CHPs salient features for electronic heat dissipation, but the main limitation of CHPs results from termination of a normal capillary flow [6,7]. When heat flux continuously increases in the evaporator side, liquid–vapor interface radius eventually reaches its minimum value and the capillary force simultaneously reaches its peak value. To maintain a normal liquid flow within the wick structure, total pressure head loss should never surpass the maximum capillary pressure.

To avoid the inherent limitations of conventional heat pipes, a new type of heat pipes known as oscillating heat pipes or pulsating heat pipes (OHPs or PHPs) were invented and patented by Akachi et al. in 1990s [5,8]. Similar to CHPs, this new type of heat pipes also employs working fluid flow and phase change to transfer heat, but it works in a different way. Fig. 1(a) shows a typical tubular OHP that is often used in experiments. A tubular OHP consists of a long wickless capillary tube bent into many turns meandering in a plain, an evaporator and a condenser located at two opposite ends, and an adiabatic region located in between. A chosen working fluid (e.g. water, acetone, or ammonia) is filled into the tube with a designated liquid–vapor ratio. The inner tube diameter must be sufficiently small (ranging from 0.1 mm to 5 mm) so that the capillary force is significant enough to counteract the gravity and hence the liquid and vapor can be discretized into separated liquid and vapor slugs (instead of stratifying into liquid and vapor layers as in CHPs) [9]. Without any external mechanical excitation, an OHP employs phase change heat transfer and forced convection to efficiently convey heat from the evaporator to the condenser through a self-excited oscillation. Each oscillating liquid slug leaves a thin film on the tube wall as it moves along the tube. Because the thickness of the thin film is very small and hence has a low thermal resistance, it can be easily evaporated at the evaporator section. When the liquid films are evaporated into the adjacent vapor slugs, the masses and pressures of the vapor slugs increase. On the other hand, when a vapor slug of high temperature and high pressure moves to the condenser section, condensation takes place and a thin liquid film forms on the tube wall resulting in decreases of the vapor slug's pressure and mass. The capillary force formed between the thin film and the adjacent liquid slugs will pump the liquid in the thin film to join the adjacent liquid slugs. The time-varying pressure difference between the high pressure of vapor slugs in the evaporator and the low pressure of vapor slugs in the condenser pushes liquid slugs to oscillate and move toward the condenser.

Although an OHP is simply constructed with only a meandering capillary tube charged with a proper working fluid, it bears many advantages that enable extraordinary heat transfer characteristics. Compared with CHPs, the outstanding features of OHPs include low pressure drop, high driving force for oscillation, high heat transfer coefficient, and low manufacturing cost. Because an OHP uses no wicking structures to return the condensate back to the evaporator, the pressure drop within the working fluid is very small. Moreover, because vapor and liquid slugs are moving in the same direction, the pressure drop due to unwanted friction force between the liquid and vapor flows does not exist. A CHP is merely driven by the capillary force from a wicking structure, but an OHP is driven primarily by the pressure difference between the heated vapor slugs and the cooled vapor slugs. The thermally driven oscillating fluid slugs inside the capillary tube will continuously sweep the tube wall, leave thin films on the tube wall, and significantly promote heat transfer through thin film evaporation

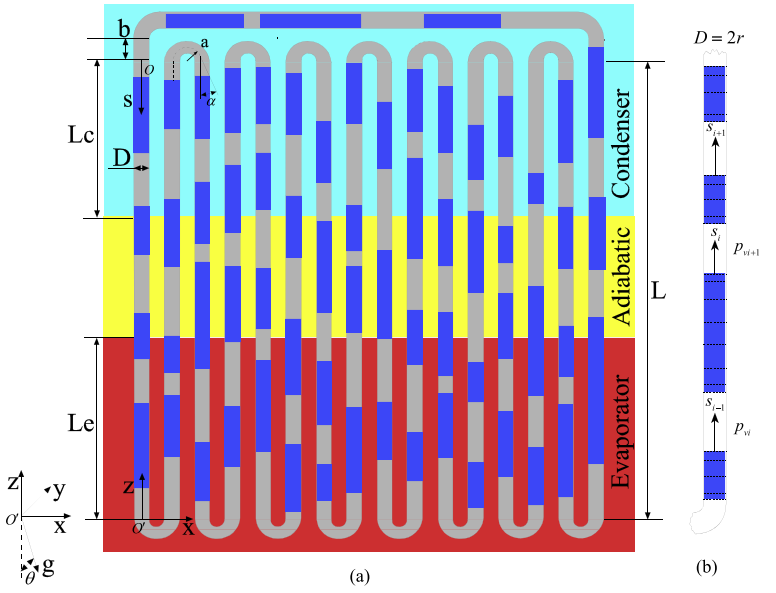

Fig. 1. A multi-turn OHP: (a) coordinate systems, and (b) numbering and finite-element discretization of fluid and vapor slugs.

and condensation. In addition to this phase change heat transfer, the forced convection due to the oscillation and circulation of fluid slugs within the tube can effectively remove the heat added at the evaporator [2]. As the input power increases, the frequency and amplitude of oscillation inside the capillary tube increase significantly and in turn dramatically promote the forced convection and the heat transfer capability. On the other hand, the highest input power for conventional heat pipes is limited by several limitations [10–12]. Without the use of delicate and expensive wicking structures that require special manufacturing techniques for CHPs, OHPs are simply made of looped tubes containing cheap working fluid, which bestows on OHPs a large commercial value. Due to its potentially high heat transfer capacity, fast thermal response, and simple and cheap construction, OHPs will certainly play an important role in electronic cooling. Hence, OHPs are sure to draw attentions from both researchers and thermal management industries.

Because of the promising heat transfer capability of OHPs, extensive experimental and theoretical studies have been conducted in recent years to explore the working mechanism of OHPs. Experimental studies often focus on the temperature variations of the condenser using thermocouples and the visualization of the working fluid flow using a high-speed camera [13] or neutron radiography [14], and theoretical studies often focus on mathematical modeling of liquid slugs' motion and vapor slugs' thermodynamic performance. Extensive experimental results on OHPs about different influential factors are reported in recent years, including the operation mode, inclination angle, number of turns, working fluids, charging ratio, gravitational force, and channel size and geometry. In 1996, Akachi et al. [15] performed experiments on open-looped circular OHPs and concluded that the thermal resistance was independent of the heat input and the inclination angle if an OHP had more than 80 turns. However, Khandekar et al. [16] stated in 2002 that the performance of OHPs depended on the orientation, charging ratio and cross section geometry. In 2003, Khandekar et al. [17] concluded that the horizontal operation mode did not work, and Maezawa et al. [18] stated in 1996 that the bottom heat mode was much better than the top heat mode. However, based on experiments on an OHP with 40 circular parallel channels and using acetone as the working fluid, Lin et al. [19] concluded that the horizontal mode had better performance. The properties of working fluid and the filling ratio are generally accepted as important factors that significantly affect the performance of OHPs. However, different values for the optimum filling ratio and the heat transfer capability of OHP have been reported. Various optimum charging ratios ranging from 20% to 70% have been reported with respect to different working fluids and operation modes. Khandekar et al. [17] reported in 2003 that the optimum charging ratio for water, ethanol and R-123 was 30%, 20% and 50%, but Miyazaki and Akachi [20] reported in 1996 that the optimized charging ratio for bottom and top heat modes was 70% and 35%, respectively. Most of contemporary investigations considered the regular gravity g as a minor factor in the design of OHPs, but Kiseev and Zolkin [21] reported in 1999 that, if an applied acceleration was increased from -6 g to 12 g, the evaporator temperature could increase by 30%. Experimental results showed that there exists an onset temperature for the oscillation of OHPs, and the heating mode, gravitational force, initial working fluid temperature, capillary tube inner diameter, filling ratio, and physical properties of working fluids all have profound influences on the heat transfer performance of OHPs. But how these factors affect performance of OHPs and what is the working mechanism of OHPs are still not fully understood.

Because of chaotic dynamic characteristics of OHPs and inherent difficulty in probing the thermodynamic process of vapor slugs, the number of proposed theoretical models is relatively small compared with the number of opulent experimental works. In 1998, based on the assumption of a continuous void fraction, Miyazaki and Akachi [22] derived a wave equation and a progressive wave solution for a closed-loop channel and a standing wave for a closed-end channel were obtained. One year later in 1999, Hosoda et al. [23] proposed a numerical solution of 1-D liquid and vapor flow by neglecting the thin liquid film, pressure drop at bends and viscous dissipation. Their numerical results showed an optimal charging ratio of 60%. In 2001, Shafii et al. [9] solved the mass, momentum and energy equations of liquid and vapor slugs under the assumption that each vapor slug is an ideal gas, each liquid slug is incompressible, and pressure losses at bends are negligible. They concluded that 95% of the heat transfer is due to sensible heat, the latent heat transfer mainly serves to provide the driving force for oscillation, and influence of gravity on the fluid oscillation is insignificant. In 2002, Zhang and Faghri [24] examined the thin film condensation and evaporation within an OHP tube wall by taking the surface tension effect into consideration. The moving effect of liquid slug was not incorporated into the model when solving the momentum equation, and the vapor was assumed to be saturated and isothermal. They indicated that the surface tension had little influence on the frequency and amplitude of oscillation. In the same year, Zhang et al. [25] simplified the model of meandering OHPs to a three-slug U-shaped miniature tube and considered it as the building block of a looped OHP. They solved the mass, momentum and energy equations for the only liquid slug and two adjacent vapor slugs using an implicit numerical method. Influences of the initial position, gravity, temperature difference between the evaporator and the condenser, and the heat transfer coefficient were investigated. Zhang and Faghri [26] also presented an OHP model with two closed ends and arbitrary number of turns, and their results showed that the oscillation amplitude and frequency were not affected by the number of turns if five turns or less are utilized in the model. Obviously, many of these numerical and experimental results are inconsistent or even contradictory to each other. This indicates that the actual working mechanism and efficiency of OHPs are still unknown.

This work is to develop a continuum-based thermomechanical theory and a nonlinear finite element model that can reveal the actual working mechanism and predict the self-excited oscillation and heat transfer performance of OHPs. The model will account for the effects of operating temperature, temperature difference between the evaporator and the condenser, fluid filling ratio, random sizes of fluid and vapor slugs, properties of working fluid, tube dimensions, number of turns, open or closed designs, gravity, surface tension, and pressure loss due to tube bending on the performance of OHPs. Moreover, advanced time–frequency analysis will be used to characterize dynamic responses of OHPs obtained from nonlinear finite element simulations and to reveal the actual working mechanisms of OHPs. The developed, general nonlinear finite-element model and the revealed working mechanisms can be used to resolve fundamental design issues and to perform design optimization of OHPs.

2. Governing equations

2.1. Equations of motion

Fig. 1(a) shows a typical multi-turn tubular OHP with a bottom heating mode. The origin of the curvilinear coordinate s is defined at Point O. The Cartesian coordinate system xyz is placed at the bottom of the OHP with the origin O' at the beginning of the first turn. In order to study the influence of gravitation, the gravity g is assumed to be on the yz plane and having an angle θ with respect to the z axis. The length from Point O to the condenser-adiabatic interface is L_c, and the one from Point O' to the evaporator-adia-

batic interface is L_e. The inner diameter of the capillary tube and the turn radius are denoted as D and a, respectively. Liquid slugs are colored in blue and each liquid slug is driven by the pressure difference between its two adjacent vapor slugs. The vapor and liquid slugs are numbered as shown in Fig. 1(b). Because the pressures of vapor slugs change with time, motions of liquid slugs are always transient. Gravity pulls a liquid slug forward or backward when the liquid slug moves in the same or opposite direction of the gravity. The gravity effect disappears when a liquid slug moves horizontally (i.e., the x direction). The pressure loss at the bending area is significant when the number of turns is large and hence should be included in the physical model. The frictional force also becomes large in a multi-turn OHP because the contact area between the liquid slugs and the capillary tube wall is large. If n liquid slugs and n vapor slugs are alternatively distributed along the tube, we obtain from Newton's second law and Fig. 1(b) that

$$\begin{aligned} &AL_{li}\rho_l\ddot{s}_i = A(p_{vi}-p_{vi+1}-\Delta p_{bi})+AL_{li}\rho_l g_i - L_{li}D\pi\tau_p,\ \ i=1,2,\ldots n-1\\ &AL_{ln}\rho_l\ddot{s}_n = A(p_{vn}-p_{v1}-\Delta p_{bn})+AL_{ln}\rho_l g_n - L_{ln}D\pi\tau_p \end{aligned} \tag{1}$$

where A is the inner cross-sectional area of the tube, L_{li} is the ith liquid slug's length, ρ_l is the density of the working fluid, s_i is the ith liquid slug's displacement along the tube with respect to its initial location (see Fig. 1(b), $s_i = 0$ when time $t = 0$), and $\ddot{s}_i \equiv d^2 s_i/dt^2$. Fig. 1(b) shows that $p_{vi}$is the vapor pressure of the ith vapor slug and the vapor pressure difference at the two ends of the ith liquid slug is $p_{vi} - p_{vi+1}$. The bending pressure loss of the ith liquid slug is assumed to be proportional to the length of the liquid slug in the bending area and denoted by Δp_{bi}. By using an empirical bending pressure loss coefficient c_b and assuming the length of the ith liquid slug in the bending area to be L_{bi}, the bending pressure loss can be presented as

$$\Delta p_{bi} = \frac{L_{bi}}{L_{li}} sign(\dot{s}_i) c_b \rho_l \dot{s}_i^2/2 \tag{2}$$

where $\dot{s}_i$ is the velocity of the ith liquid slug. The pressure loss of a vapor slug is much smaller than that of a liquid slug and is not considered here. The effective gravity g_i on the ith liquid slug is defined as the gravity component along the positive direction of s_i. If the ith liquid slug is located at the first turn in the condenser area and the angle between the velocity $\dot{s}_i$ and the -z axis is α(see Fig. 1(a)), the effective gravity g_i on the ith liquid slug is given by

$$g_i = \frac{g\cos\theta \int_0^{L_{li}} \cos\alpha\ ds}{L_{li}} \tag{3}$$

where θ is the inclination angle of the OHP. If a liquid slug moves upward along the capillary tube, i.e.,$\alpha = 180\,^\circ$, the effective gravitational acceleration g_i is equal to $-g\cos\theta$. The shear stress τ_p on the ith liquid slug can be obtained as

$$\tau_p = \frac{8\mu_l u_m}{D} = \frac{8\mu_l}{D}\dot{s}_i \tag{4}$$

where μ_l is the dynamic viscosity, u_m is the averaged velocity of the liquid slug, and the flow in the capillary tube is assumed to be laminar. Substituting Eqs. (2) and (4) into Eq. (1) yields the following governing dynamic equations of the liquid slugs:

$$\begin{cases} L_{l1}\rho_l\ddot{s}_1 = p_{v1}-p_{v2}-\frac{L_{b1}}{L_{l1}}sign(\dot{s}_1)c_b\rho_l\dot{s}_1^2/2 + L_{l1}\rho_l g_1 - \frac{32\mu_l L_{l1}}{D^2}\dot{s}_1 \\ L_{l2}\rho_l\ddot{s}_2 = p_{v2}-p_{v3}-\frac{L_{b2}}{L_{l2}}sign(\dot{s}_2)c_b\rho_l\dot{s}_2^2/2 + L_{l2}\rho_l g_2 - \frac{32\mu_l L_{l2}}{D^2}\dot{s}_2 \\ \vdots \\ L_{ln}\rho_l\ddot{s}_n = p_{vn}-p_{v1}-\frac{L_{bn}}{L_{ln}}sign(\dot{s}_n)c_b\rho_l\dot{s}_n^2/2 + L_{ln}\rho_l g_n - \frac{32\mu_l L_{ln}}{D^2}\dot{s}_n \end{cases} \tag{5}$$

2.2. Thermodynamics of vapor slugs

Thin liquid films left on the tube wall by liquid slugs evaporate into vapor slugs and increase the total enthalpy of the system. On the other hand, a vapor slug in the condenser section condenses to the tube wall and adds to the mass of adjacent liquid slugs. Following this line of reasoning, one can conclude that each vapor slug is an open thermodynamic system that exchanges mass with surrounding liquid slugs. Because every vapor slug going through the evaporator and condenser sections undergoes a similar thermodynamic process, we choose the ith vapor slug for investigation. A general form of the energy conservation law for an open system can be presented as

$$\begin{aligned} \dot{Q} = {} & dE_{cv}/dt + \dot{W}_{net} + \sum (h + \dot{s}^2/2 + gz)_{out}\dot{m}_{out} \\ & - \sum (h + \dot{s}^2/2 + gz)_{in}\dot{m}_{in} \end{aligned} \tag{6}$$

where $\dot{Q}, dE_{cv}/dt$ and $\dot{W}_{net}$ are the heat transfer rate into the open system, the internal energy increase rate of the open system, and the mechanical power done by the system to the environment. Moreover, $\sum (h + \dot{s}^2/2 + gz)_{out}\dot{m}_{out}$ and $\sum (h + \dot{s}^2/2 + gz)_{in}\dot{m}_{in}$ are energy exchanged between the system and the environment due to the mass flow, h represents the specific enthalpy, $\dot{s}^2/2$ is the specific kinetic energy, and gz represents the specific gravitational potential energy.

Because most of heat is transferred between liquid and the wall either by thin film evaporation or forced convection, one can assume that heat transfer directly between a vapor slug and wall can be neglected, i.e., $\dot{Q}$ equals zero. We assume the thin film on the tube wall absorbs energy and evaporates into the vapor slug, and the total enthalpy of the vapor slug increases. On the other hand, the total enthalpy of the vapor slug decreases in the condenser section. Because the vapor mass density is negligibly small (typically only 0.1% of the liquid mass density), the changes of kinetic and potential energy is not significant compared to the change of enthalpy. For a vapor slug, the oscillating motion excited by the thermal energy added to the OHP produces compression and expansion. During the compression/expansion process, because the pressure wave propagation is much faster than the heat transfer process, a vapor slug's expansion/compression process in an OHP can be assumed to be adiabatic. Hence, the relation between the vapor temperature and pressure can be expressed as

$$T_{vi} = \frac{A}{C_i R} p_{vi}^{(\gamma-1)/\gamma} \Longleftrightarrow p_{vi} = \left(\frac{C_i R}{A} T_{vi}\right)^{\gamma/(\gamma-1)}, \quad i = 1,2,\ldots,n \tag{7}$$

where $\gamma(\equiv c_p/c_v)$ is the heat capacity ratio, c_v and c_p are the isochoric and isobaric specific heats (i.e., heat capacities) of the working fluid's vapor, A is the cross-sectional area of the vapor slug, T_{vi} and p_{vi} are temperature and pressure of the ith vapor slug, and R is the specific gas constant of the working fluid. The integration constant C_i in Eq. (7) can be obtained through a referential state

$$C_i = \frac{A}{RT_0} p_0^{(\gamma-1)/\gamma} \tag{8}$$

where p_0 and T_0 are chosen as the ith vapor slug's initial pressure and temperature. If the initial pressure and temperature of every vapor slug are the same, the integration constants in Eq. (8) are the same for all vapor slugs. It follows from the ideal gas law and Fig. 1(b) that

$$p_{vi}A(s_i - s_{i-1} + L_{vi}) = m_{vi}RT_{vi} \tag{9}$$

where m_{vi} is the mass of the ith vapor slug,s_i and s_{i-1} are the displacements of the ith and (i-1) th liquid slugs, and L_{vi} is the initial length of the ith vapor slug. Substituting Eq. (9) into Eq. (7) yields the relationship between the vapor mass and pressure as

$$m_{vi} = C_i(s_i - s_{i-1} + L_{vi})p_{vi}^{1/\gamma} \Longleftrightarrow p_{vi} = \left[\frac{m_{vi}}{C_i(s_i - s_{i-1} + L_{vi})}\right]^{\gamma} \quad \text{for } i = 2,3\ldots,n \tag{10}$$

For $i = 1$, Eq. (10) should be modified to be

$$m_{v1} = C_1(s_1 - s_n + L_{v1})p_{v1}^{1/\gamma} \Longleftrightarrow p_{v1} = \left[\frac{m_{v1}}{C_1(s_1 - s_n + L_{v1})}\right]^{\gamma} \tag{11}$$

where s_1 and s_n represent the displacements of the first and last liquid slugs.

2.3. Heat transfer between vapor slugs and the tube wall

When a liquid slug moves into the evaporator region, a thin film will be left behind on the tube wall. The thin film absorbs heat from the heater, evaporates into its adjacent vapor slug, and increases the mass and enthalpy of the vapor slug. When this high-temperature, high-pressure vapor slug moves to the condenser region, film condensation occurs. When a vapor slug goes through the adiabatic region, there is no heat transfer between the vapor slug and the tube wall. If heat transfer coefficients between the vapor slug and the tube wall in the evaporator and condenser regions are assumed to be h_e and h_c, the mass increase rate of the ith vapor slug can be assumed to be

$$\dot{m}_{vi} = \pi D[L_{ie}(T_e - T_{vi})h_e - L_{ic}(T_{vi} - T_c)h_c]/h_{fg}, \quad i = 1,2,3,\ldots,n \tag{12}$$

where h_{fg} is the latent heat of the working fluid, $\dot{m}_{vi}$ is the mass increase rate of the ith vapor slug, $L_{ie}(L_{ic})$ is the ith vapor slug's partial length in contact with the evaporator (condenser), T_{vi} is the ith vapor slug's temperature, and $T_e(T_c)$ is the temperature of the evaporator (condenser). The phase-change heat transfer coefficient h_e and h_c can be estimated using Chen's model shown later in Eq. (31).

3. Modal analysis

Modal analysis is excellent for understanding a complex system's dynamic characteristics because it provides the system's natural frequencies and modal shapes under small-amplitude free vibration. Although an OHP is typically taken as a heat transfer device, it is also a mass-spring mechanical system of multiple degrees of freedom (DOF) and hence modal analysis is useful for revealing its dynamic properties. If the bending pressure loss and gravity are neglected, Eq. (5) is simplified to be

$$\begin{cases} L_{l1}\rho_l\ddot{s}_1 + \frac{32\mu_l L_{l1}}{D^2}\dot{s}_1 = p_{v1} - p_{v2} \\ L_{l2}\rho_l\ddot{s}_2 + \frac{32\mu_l L_{l2}}{D^2}\dot{s}_2 = p_{v2} - p_{v3} \\ \vdots \\ L_{ln}\rho_l\ddot{s}_n + \frac{32\mu_l L_{ln}}{D^2}\dot{s}_n = p_{vn} - p_{v1} \end{cases} \tag{13}$$

Rewriting Eq. (13) in matrix form yields

$$\begin{bmatrix} L_{l1}\rho_l & & & 0 \\ & L_{l2}\rho_l & & \\ & & \ddots & \\ 0 & & & L_{ln}\rho_l \end{bmatrix} \begin{Bmatrix} \ddot{s}_1 \\ \ddot{s}_2 \\ \vdots \\ \ddot{s}_n \end{Bmatrix} + \begin{bmatrix} 32\mu_l L_{l1}/D^2 & & & 0 \\ & 32\mu_l L_{l2}/D^2 & & \\ & & \ddots & \\ 0 & & & 32\mu_l L_{ln}/D^2 \end{bmatrix} \times \begin{Bmatrix} \dot{s}_1 \\ \dot{s}_2 \\ \vdots \\ \dot{s}_n \end{Bmatrix} = \begin{bmatrix} 1 & -1 & & \\ & 1 & -1 & \\ & & \ddots & \ddots \\ & & & 1 & -1 \\ -1 & & & & 1 \end{bmatrix} \begin{Bmatrix} p_{v1} \\ p_{v2} \\ \vdots \\ p_{vn-1} \\ p_{vn} \end{Bmatrix} \tag{14}$$

Eqs. (10) and (11) show the relationships between vapor pressures and displacements of liquid slugs. Taking derivatives on both sides of both equations gives the following relationships

$$\begin{aligned} dp_{vi} &= \frac{\gamma p_{vi}}{L_{vi}} d(s_{i-1} - s_i) \text{ for } i = 2,3,\ldots,n \\ dp_{v1} &= \frac{\gamma p_{v1}}{L_{v1}} d(s_n - s_1) \end{aligned} \tag{15}$$

where $s_i - s_{i-1} + L_{vi} \approx L_{vi}$ is assumed because modal analysis is under the assumption of small-amplitude vibration. Rewriting Eq. (15) in matrix form yields

$$\begin{Bmatrix} dp_{v1} \\ dp_{v2} \\ dp_{v3} \\ \vdots \\ dp_{vn} \end{Bmatrix} = \begin{bmatrix} -\gamma p_{v1}/L_{v1} & 0 & 0 & \cdots & \gamma p_{v1}/L_{v1} \\ \gamma p_{v2}/L_{v2} & -\gamma p_{v2}/L_{v2} & 0 & \cdots & 0 \\ 0 & \gamma p_{v3}/L_{v3} & -\gamma p_{v3}/L_{v3} & & \vdots \\ \vdots & \cdots & & & 0 \\ 0 & \cdots & 0 & \gamma p_{vn}/L_{vn} & -\gamma p_{vn}/L_{vn} \end{bmatrix} \times \begin{Bmatrix} ds_1 \\ ds_2 \\ ds_3 \\ \vdots \\ ds_n \end{Bmatrix} \Longleftrightarrow \{dp_v\} = [S]\{ds\} \tag{16}$$

where $[S]$ describes the spring effect of vapor slugs. Moreover, because p_v and L_v change with time, this liquid–vapor system is an inherently nonlinear dynamical system and its nature frequencies are not constant. Linear modal analysis gives the nature frequencies and modal shapes of the system under the assumption that relationships between vapor pressures and fluid slugs' displacements are linear. If $(\bar{s}_i, \bar{p}_{vi})$ represents an equilibrium state at a specific time, we define

$$s_i \equiv \bar{s}_i + ds_i, \;\; p_{vi} \equiv \bar{p}_{vi} + dp_{vi} \text{ for } i = 1,\ldots,n \tag{17}$$

Substituting Eq. (17) into Eq. (14) and using Eq. (16) yields

$$[M]\{d\ddot{s}\} + [C]\{d\dot{s}\} + [\widehat{K}]\{ds\} = \{0\} \tag{18}$$

where the mass matrix $[M]$, damping matrix $[C]$ and tangent stiffness matrix $[\widehat{K}]$ are given by

$$[M] = \begin{bmatrix} L_{l1}\rho_l & & & 0 \\ & L_{l2}\rho_l & & \\ & & \ddots & \\ 0 & & & L_{ln}\rho_l \end{bmatrix}, \quad [C] = \begin{bmatrix} 32\mu_l L_{l1}/D^2 & & & 0 \\ & 32\mu_l L_{l2}/D^2 & & \\ & & \ddots & \\ 0 & & & 32\mu_l L_{ln}/D^2 \end{bmatrix},$$

$$[\widehat{K}] = \begin{bmatrix} -1 & 1 & & & \\ & -1 & 1 & & \\ & & \ddots & \ddots & \\ & & & -1 & 1 \\ 1 & & & & -1 \end{bmatrix} \begin{bmatrix} -\gamma p_{v1}/L_{v1} & 0 & 0 & \cdots & \gamma p_{v1}/L_{v1} \\ \gamma p_{v2}/L_{v2} & -\gamma p_{v2}/L_{v2} & 0 & \cdots & 0 \\ 0 & \gamma p_{v3}/L_{v3} & -\gamma p_{v3}/L_{v3} & \cdots & 0 \\ \vdots & \cdots & \vdots & \ddots & \vdots \\ 0 & \cdots & 0 & \gamma p_{vn}/L_{vn} & -\gamma p_{vn}/L_{vn} \end{bmatrix} \tag{19}$$

When a mechanical system is subject to a small external excitation, its vibration amplitude becomes excessively large when the excitation frequency is close to some specific values. This phenomenon is known as *resonance* and the specific frequencies are called *resonant* or *natural frequencies* of the system. When a system is under an excitation at a resonant frequency, each DOF moves harmonically at the excitation frequency with a 0 ° or 180 ° phase angle with respect to other DOFs, and the corresponding geometric relation between different DOFs is called the mode shape. A linear dynamical system's response to an arbitrary excitation is always a combination of many modal vibrations of the system. Modal analysis is to obtain natural frequencies and modal shapes of a system through eigenvalue analysis. Under free

undamped vibration, the slug-flow model becomes a simple mass-spring system governed by

$$[M]\{d\ddot{s}\} + [\widehat{K}]\{ds\} = \{0\} \tag{20}$$

In linear modal analysis, the tangential stiffness matrix $[\widehat{K}]$ at a specified time is assumed to remain constant under small oscillation. The liquid slugs are assumed to oscillate harmonically and therefore we have

$$\{ds\} = \{\phi\}\sin(\omega t) \tag{21}$$

Substituting Eq. (21) into Eq. (20) yields

$$([\widehat{K}] - \omega^2[M])\{\phi\} = 0 \tag{22}$$

Because $|[\widehat{K}] - \omega^2[M]| = 0$ is necessary for Eq. (22) to have non-zero eigenvectors $\{\phi\}$, the natural frequencies $\omega_i (i = 1, \ldots, n)$ can be obtained by solving the algebraic equation $|[\widehat{K}] - \omega^2[M]| = 0$. The ith mode shape $\{\phi\}_i$ is calculated by substituting the so-obtained natural frequency ω_i back into Eq. (22).

4. Transient analysis

Because modal analysis is to obtain a mechanical system's dynamic characteristics under free undamped vibrations, heat transfer between the tube wall and liquid and vapor slugs, gravity, viscosity-induced damping, and bending-induced pressure drop are not included in modal analysis of OHPs. The heat transfer between the tube wall and vapor and fluid slugs serves as the driving force for slug oscillation and therefore is important for evaluating the heat transfer capability of an OHP. Because the driving force is determined by a complex combination of time-varying lengths and pressures of vapor slugs, physical properties of the working fluid, fluid filling ratio, the heating mode (top or bottom) and others, transient analysis is necessary in order to account for all of these factors in evaluating the performance of an OHP.

For transient analysis of an OHP, the governing equations of motion need to include all the heat transfer effects between the tube wall and fluid and vapor slugs, gravity, viscosity-induced damping, and bending-induced pressure drop by following Eq. (5) as

$$[M]\{\ddot{s}\} + [C]\{\dot{s}\} + [K]\{s\} = \{R\} \tag{23}$$

where the mass matrix $[M]$, the damping matrix $[C]$, the stiffness matrix $[K]$, and the load vector $\{R\}$ are defined as

$$[M] = \begin{bmatrix} L_{l1}\rho_l & & & 0 \\ & L_{l2}\rho_l & & \\ & & \ddots & \\ 0 & & & L_{ln}\rho_l \end{bmatrix},\quad [C] = \begin{bmatrix} 32\mu_l L_{l1}/D^2 & & & 0 \\ & 32\mu_l L_{l2}/D^2 & & \\ & & \ddots & \\ 0 & & & 32\mu_l L_{ln}/D^2 \end{bmatrix}$$

$$[K]\{s\} \equiv -\begin{Bmatrix} p_{v1} - p_{v2} \\ p_{v2} - p_{v3} \\ \vdots \\ p_{vn-1} - p_{vn} \\ p_{vn} - p_{v1} \end{Bmatrix},\quad \{R\} = \begin{Bmatrix} L_{l1}\rho_l g_1 - sign(\dot{s}_1)c_b\rho_l\dot{s}_1^2 L_{b1}/(2L_{l1}) \\ L_{l2}\rho_l g_2 - sign(\dot{s}_2)c_b\rho_l\dot{s}_2^2 L_{b2}/(2L_{l2}) \\ \vdots \\ L_{ln}\rho_l g_n - sign(\dot{s}_n)c_b\rho_l\dot{s}_n^2 L_{bn}/(2L_{ln}) \end{Bmatrix} \tag{24}$$

Note that the explicit form of $[K]$ is not available because the relationships between the vapor slugs' pressures and the displacements of fluid slugs shown by Eqs. (10) and (11) are implicit and highly nonlinear.

Eq. (23) will be solved using a modified Euler predictor–corrector method [27]. We move the $[K]\{s\}$ to the right side and treat it as a part of the load vector as

$$[M]\{\ddot{s}\} + [C]\{\dot{s}\} = \{F\}, \quad \{F\} \equiv \{R\} - [K]\{s\} \tag{25}$$

By defining $\{\beta\} \equiv \{\dot{s}\}$ Eq. (25) can be written into the following $2n$ first-order ordinary differential equations:

$$\begin{aligned} &\{\dot{s}\} - \{\beta\} = \{0\} \\ &[M]\{\dot{\beta}\} + [C]\{\beta\} = \{F\} \end{aligned} \tag{26}$$

Because Eqs. (10) and (11) show that the vapor masses m_{vi} (and hence p_{vi}) are implicit time-varying functions of $\{s\}$, Eqs. (12) and (26) need to be solved simultaneously. Combining Eqs. (12) and (26) in matrix form yields

$$[\widetilde{C}]\{\dot{D}\} + [\widetilde{K}]\{D\} = \{\widetilde{F}\} \tag{27}$$

where $\{D\}$, $[\widetilde{C}]$, $[\widetilde{K}]$ and $\{\widetilde{F}\}$ are defined as

$$\{D\} \equiv \begin{Bmatrix} \{s\} \\ \{\beta\} \\ \{m\} \end{Bmatrix}_{3n\times 1},\quad \{m\} \equiv \begin{Bmatrix} m_{v1} \\ \vdots \\ m_{vn} \end{Bmatrix},\quad [\widetilde{C}] \equiv \begin{bmatrix} [I] & [0] & [0] \\ [0] & [M] & [0] \\ [0] & [0] & [I] \end{bmatrix}_{3n\times 3n},$$

$$[\widetilde{K}] = \begin{bmatrix} [0] & -[I] & [0] \\ [0] & [C] & [0] \\ [0] & [0] & [0] \end{bmatrix}_{3n\times 3n}$$

$$\{\widetilde{F}\} = \begin{Bmatrix} \begin{Bmatrix} 0 \\ \vdots \\ 0 \end{Bmatrix} \\ \begin{Bmatrix} L_{l1}\rho_l g_1 - sign(\dot{s}_1)c_b\rho_l\dot{s}_1^2 L_{b1}/(2L_{l1}) + p_{v1} - p_{v2} \\ \vdots \\ L_{ln}\rho_l g_n - sign(\dot{s}_n)c_b\rho_l\dot{s}_n^2 L_{bn}/(2L_{ln}) + p_{vn} - p_{v1} \end{Bmatrix} \\ \begin{Bmatrix} \pi D[L_{1e}(T_e - T_{v1})h_e - L_{1c}(T_{v1} - T_c)h_c]/h_{fg} \\ \vdots \\ \pi D[L_{ne}(T_e - T_{vn})h_e - L_{nc}(T_{vn} - T_c)h_c]/h_{fg} \end{Bmatrix} \end{Bmatrix} \tag{28}$$

where [0] is a $n \times n$ null matrix and $[I]$ is a $n \times n$ identity matrix. Eq. (27) can be solved using a modified Euler Predictor–Corrector method with convergence check at every time step [27].

5. Finite-element analysis of the heat transfer in liquid slugs

When a liquid slug oscillates within the capillary tube, a laminar flow with a large radial temperature gradient is formed and a large amount of heat is transferred by radial conduction. Meanwhile, the non-uniform radial heat transfer along the liquid slug also promotes the axial heat transfer. Moreover, the fluid slug's two neighboring vapor slugs of different temperatures also affect its axial heat transfer. Because a typical capillary tube's inner diameter commonly ranges from 0.1 mm to 5 mm and is much smaller than the liquid slug's length, heat transfer in a liquid slug can be simplified into a 1-D model. Fig. 2 schematically shows how energy balances within a differential liquid element. With a moving coordinate y defined with an origin fixed at the top liquid–vapor interface, a mathematical form of the energy conservation process within a differential liquid element is given by

$$c_{pl}\rho_l\dot{T}_l = k_l T_{lyy} + \frac{4h_l}{D}(T_w - T_l) \tag{29}$$

where $\dot{T}_l = \partial T_l/\partial t$, $T_{lyy} = \partial^2 T_l/\partial y^2$, and c_{pl}, k_l and ρ_l are respectively the isobaric specific heat, thermal conductivity and density of the working fluid under a working temperature T_l. The tube wall temperature is T_W. The convective term is neglected because the diameter of the capillary tube is very small and hence the radial heat transfer between the tube wall and the liquid slug is much stronger than the axial heat transfer. Moreover, the convection within the liquid slug is weak due to the limited small space.

The heat transfer coefficient of a train of liquid and vapor slugs in a capillary tube with phase change for unidirectional flow was

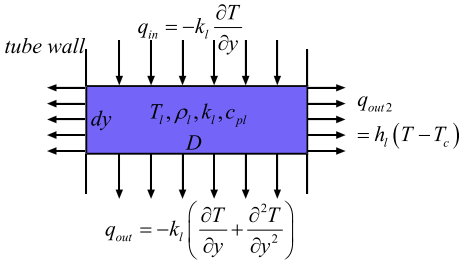

Fig. 2. Conservation of energy within a differential liquid element.

estimated by Ma et al. [2]. The total heat transfer coefficient can be expressed as

$$h = h_e + h_l \tag{30}$$

where h_e is the nucleate boiling heat transfer coefficient (phase change heat transfer coefficient in Eq. (12)) and h_l is the bulk convection heat transfer coefficient caused by oscillating motion. According to Chen's model [28], h_e can be calculated as

$$h_e = 0.00122 \left[\frac{k_l^{0.79} c_{pl}^{0.45} \rho_l^{0.49}}{\sigma^{0.5} \mu_l^{0.29} h_{gf}^{0.24} \rho_v^{0.24}} \right] [T_w - T_{sat}(P_l)]^{0.24} [P_{sat}(T_w) - P_l]^{0.75} S \tag{31}$$

where σ and ρ_v are the surface tension coefficient of the working fluid and vapor density, and the suppression factor S is a function of the two-phase Reynolds number Re_{tp} given by

$$S = (1 + 2.56 \times 10^{-6} Re_{tp}^{1.17})^{-1} \tag{32}$$

The two-phase Reynolds number in Eq. (32) can be calculated by

$$Re_{tp} = Re_l [F(X_{tt})]^{1.25} \tag{33}$$

where the liquid Reynolds number Re_l and the Martinelli parameter X_{tt} are defined as

$$Re_l = \frac{G(1-x)D}{\mu_l} \tag{34}$$

$$X_{tt} = \left(\frac{1-x}{x} \right)^{0.9} \left(\frac{\rho_v}{\rho_l} \right)^{0.5} \left(\frac{\mu_l}{\mu_v} \right)^{0.1} \tag{35}$$

The mass flux G in Eq. (34) is defined as $G = \bar{u}\bar{\rho}$ where $\bar{u}$ and $\bar{\rho}$ are the average velocity and density of the two phase flow. The function $F(X_{tt})$ depends on the Martinelli parameter as

$$\begin{aligned} &F(X_{tt}) = 1 \text{ for } X_{tt}^{-1} \leqslant 0.1 \\ &F(X_{tt}) = 2.35 \left(0.213 + \frac{1}{X_{tt}} \right)^{0.736} \text{ for } X_{tt}^{-1} > 0.1 \end{aligned} \tag{36}$$

The quality x in Eq. (35) can be calculated by

$$x = \frac{\rho_v - r_c \rho_v}{\bar{\rho}} \tag{37}$$

where r_c is the charging ratio, and the average density of working fluid $\bar{\rho}$ can be calculated from

$$\frac{1}{\bar{\rho}} = \frac{x}{\rho_v} + \frac{1-x}{\rho_l} \tag{38}$$

The bulk convection heat transfer coefficient h_l caused by oscillating motion can be determined by applying Martinelli parameter to a two-phase flow

$$h_l = F(X_{tt}) \bar{h}_l \tag{39}$$

where $\bar{h}_l$ is the liquid-phase heat transfer coefficient determined by

$$\bar{h}_l = 0.023 \left(\frac{k_l}{D} \right) Re_l^{0.8} \mathrm{Pr}_l^{0.4} \tag{40}$$

Shao and Zhang [29] suggested that the thermal resistance at a vapor–liquid interface can be neglected and hence the vapor and liquid had the same temperature at a vapor–liquid interface. However, such a hasty assumption renders sharp temperature change at a liquid slug's two ends, which is not realistic. Hence, the following boundary conditions based on a heat transfer rate instead of temperature are proposed for Eq. (29):

$$q'' = -k_l T_{ly}|_{y=0} = h_{\delta 1} (T_{v1} - T_l|_{y=0}) \text{ at } y = 0 \tag{41}$$

$$q'' = -k_l T_{ly}|_{y=L_j} = -h_{\delta 2} (T_{v2} - T_l|_{y=L_j}) \text{ at } y = L_j \tag{42}$$

where q'' is the heat flux along the positive y direction, $h_{\delta 1}$ and $h_{\delta 2}$ are the interfacial heat transfer coefficients, $T_l|_{y=0}$ and $T_l|_{y=L_p}$ are the temperatures at the liquid slug's two ends, and L_j is the length of jth liquid slug. Schrage [30] proposed a way of estimating the heat transfer coefficient across the liquid–vapor interface through the kinetic theory of gas as

$$h_\delta = \left(\frac{2\hat{\sigma}}{2 - \hat{\sigma}} \right) \left(\frac{h_{fg}^2}{T_v v_{lv}} \right) \left(\frac{M_v}{2\pi R_u T_v} \right)^{1/2} \left(1 - \frac{p_v v_{lv}}{2 h_{fg}} \right) \tag{43}$$

$$a = \frac{q''}{\rho_v h_{fg}} \left(\frac{2RT_v}{M_v} \right)^{1/2} \tag{44}$$

where $\hat{\sigma}$ is a mass accommodation coefficient with a value between 0 and 1, indicating the ratio of vapor molecules absorbed into the liquid and all the molecules impinging on the liquid surface. Moreover, p_v, T_v and M_v are pressure, temperature and molecular weight of the given vapor at a given status, R is the universal gas constant, and $v_{lv} = v_v - v_l$ is the specific volume difference between the vapor and the liquid. The mass accommodation coefficient of liquid has been widely studied over the past eight decades and its values reported in more than 40 literatures are not consistent with each other, ranging from 0.001 to 1 [31,32]. Because of the difficulty in obtaining an accurate value for $\hat{\sigma}$ and the minor influence of the liquid–vapor interface heat transfer, a constant value of $\hat{\sigma} = 0.03$ is often used. In addition, Eq. (43) is valid only when the value of a in Eq. (44) is sufficiently low, which is true in condensation and vaporization of a commonly used working fluid. For example, a is 1.3×10^{-4} for a saturated pure water at 100 °C and condensing or vaporizing at a heat flux of 100 kW/m^2 [33].

After a finite-element model for one liquid slug is developed, one can use it for every other liquid slug with different boundary conditions and physical properties. Then, these heat transfer finite-element equations can be combined with the fluid slugs' discrete equations of motion (Eq. (27)) into the final thermomechanical model of the OHP. Applying the weighted-residual method to Eq. (29) for the jth fluid slug and integrating from $y = 0$ to $y = L_j$ yields

$$\begin{aligned} 0 &= \int_0^{L_j} \left(c_{pl} \rho_l \dot{T}_l - k_l T_{lyy} - \frac{4h_l}{D} (T_w - T_l) \right) \delta T_l dy \\ &= \sum_{i=1}^{N_{ej}} \int_0^{e_i} \left(c_{pl} \rho_l \dot{T}_l \delta T_l + k_l T_{ly} \delta T_{ly} + \frac{4h_l}{D} T_l \delta T_l - \frac{4h_l}{D} T_w \delta T_l \right) dy \\ &\quad + k_l T_{ly} \delta T_l|_{y=0} - k_l T_{ly} \delta T_l|_{y=L_j} \\ &= \sum_{i=1}^{N_{ej}} \left\{ \delta T_l^{(i)} \right\}^T \left[[c^{(i)}] \left\{ \dot{T}_l^{(i)} \right\} + [k^{(i)}] \left\{ T_l^{(i)} \right\} - \{g^{(i)}\} \right] - \{\delta T_l\}^T \{H\} \\ &= \{\delta T_l\}^T ([C]\{\dot{T}_l\} + [K]\{T_l\} - \{G\} - \{H\}) \end{aligned} \tag{45}$$

where L_j and N_{ej} are the length and total number of elements of the jth liquid slug, and e_i is the elemental length of the ith finite element for the jth liquid slug. Hence the differential equation for the jth liquid slug can be discretized into the following ODEs:

$$[C]\{\dot{T}_l\} + [K]\{T_l\} = \{G\} + \{H\} \tag{46}$$

Linear shape functions are used to interpolate the temperature profile within a finite element as:

$$\begin{aligned} T_l^{(i)} &= T_1^{(i)}N_1(y) + T_2^{(i)}N_2(y) = \{N_1(y), N_2(y)\}\begin{Bmatrix} T_1^{(i)} \\ T_2^{(i)} \end{Bmatrix} \\ &\equiv \{N\}^T\left\{T_l^{(i)}\right\} = \left\{T_l^{(i)}\right\}^T\{N\} \\ N_1(y) &= 1 - \frac{y}{e_i},\ N_2(y) = \frac{y}{e_i} \end{aligned} \tag{47}$$

where $T_l^{(i)}$ is a linear distribution of temperature in terms of the coordinate y within the ith element, and $T_1^{(i)}$ and $T_2^{(i)}$ are nodal temperatures. Because the coordinate y moves with the element, the wall temperature T_W for each element changes with time. When the ith element in the jth liquid slug moves into the condenser region, the wall temperature T_W in Eq. (45) equals the condenser temperature T_c. On the other hand, when the element moves into the evaporator region, the wall temperature $T_W$equals the evaporator temperature T_e. For the ith element, the elemental matrices $[c^{(i)}]$ and $[k^{(i)}]$ and the vector $\{g^{(i)}\}$ are given by

$$\begin{aligned} [c^{(i)}] &\equiv \int_0^{e_i} c_{pl}\rho_l\{N\}\{N\}^T dy = \tfrac{c_{pl}\rho_l e_i}{6}\begin{bmatrix} 2 & 1 \\ 1 & 2 \end{bmatrix} \\ [k^{(i)}] &\equiv \int_0^{e_i}\left(k_l\{N_y\}\{N_y\}^T + \tfrac{4h_l}{D}\{N\}\{N\}^T\right)dy \\ &= \tfrac{k_l}{e_i}\begin{bmatrix} 1 & -1 \\ -1 & 1 \end{bmatrix} + \tfrac{2h_l e_i}{3D}\begin{bmatrix} 2 & 1 \\ 1 & 2 \end{bmatrix} \\ \{g^{(i)}\} &\equiv \int_0^{e_i}\tfrac{4h_l}{D}T_w\{N\}dy = \tfrac{2h_l}{D}T_w e_i\begin{Bmatrix} 1 \\ 1 \end{Bmatrix} \end{aligned} \tag{48}$$

However, when the liquid slug moves into the insulator area, because no heat is transferred, the wall temperature T_W is equal to the liquid temperature T_l and the elemental stiffness matrix and force vector become

$$[k^{(i)}] \equiv \int_0^{e_i} k_l\{N_y\}\{N_y\}^T dy, \{g^{(i)}\} \equiv \{0\} \tag{49}$$

In addition, the concentrated forcing vector $\{H\}$ in Eq. (46) is obtained from the boundary conditions shown in Eqs. (41) and (42) as

$$\{H\} = \{h_{\delta 1}(T_{v1} - T_l|_{y=0}), 0, 0 \ldots, h_{\delta 2}(T_{v2} - T_l|_{y=L_j})\}^T \tag{50}$$

where $h_{\delta 1}$ and $h_{\delta 2}$ are the interfacial heat transfer coefficients that keep changing with physical properties of the vapor slug and therefore should be recalculated using Eq. (43) in every iteration of solving Eq. (46) using the modified Euler predictor–corrector method.

6. Heat transfer of an OHP

When the liquid slugs circulate and oscillate in the capillary tube, they absorb heat from the evaporator and release heat to the condenser. Evaporation of the liquid film and condensation of the vapor also remove some heat. A typical experimental set-up of a looped OHP consists of a cooling bath, a power supply and a data acquisition system [2]. The evaporator is a strip resistance heater that is spanned over a copper plate. The adiabatic region is insulated using a fiber-glass insulator. The heat loss in the adiabatic region is less than 1.5% based on calculation [2]. Because the current and voltage of the power supply are usually constant in experiment, the heat flux input q_e can be controlled manually. In fact, the temperature differences between different regions can be measured by multiple thermocouples. On the other hand, the temperature of the liquid in the cooling bath can be assumed to be a constant T_c. The heat transfer of a looped OHP consists of two parts: the latent heat transfer q_0 and the sensible heat transfer q_1. The total heat transferred out of the evaporator,Q_e, is given by

$$\begin{aligned} Q_e &= \int_0^t q_e dt, \quad q_e = q_{e0} + q_{e1} \\ &= \sum_{i=1}^{I_e} h_{fg}\dot{m}_{vi} + \pi D\sum_{j=1}^{J_e}\int_0^{L_{lj}} h_l(T_e - T_{lj})dy \end{aligned} \tag{51}$$

where $\dot{m}_{vi}$ is the mass changing rate of the ith vapor slug, T_{lj} is the temperature of the jth liquid slug, L_{lj} is the length of the jth liquid slug, and I_e and J_e are the total numbers of vapor and liquid slugs in the evaporator region, respectively. Similarly the total heat transferred into the condenser, Q_c, can be presented as

$$\begin{aligned} Q_c &= \int_0^t q_c dt, q_c = q_{c0} + q_{c1} \\ &= -\sum_{i=1}^{I_c} h_{fg}\dot{m}_{vi} + \pi D\sum_{j=1}^{J_c}\int_0^{L_{lj}} h_l(T_{lj} - T_c)\ dy \end{aligned} \tag{52}$$

where I_c and J_c are the numbers of vapor and liquid slugs in the condenser region. At the initial state, Q_e and Q_c are usually not equal to each other. When the average temperature of all liquid slugs reaches a steady state, $\dot{Q}_e$ should equal to $\dot{Q}_c$ because no net heat absorbed or rejected from the slug flow system. The total latent heat Q_{e0} and sensible heat Q_{e1} transferred out of the evaporator are given by

$$Q_{e0} = \int_0^t q_{e0}dt, q_{e0} = \sum_{i=1}^{I_e} h_{fg}\dot{m}_{vi} \tag{53}$$

$$Q_{e1} = \int_0^t q_{e1}dt, q_{e1} = \pi D\sum_{j=1}^{J_e}\int_0^{L_{lj}} h_l(T_e - T_{lj})dy \tag{54}$$

Shafii et al. [9] reported that the sensible heat transfer is dominant in an OHP, i.e., Q_{e1} is much larger than Q_{e0} in a steady state.

7. Simulation and characterization results

7.1. Linear modal analysis of OHPs

Modal analysis of an OHP provides its dynamic characteristics, including natural frequencies and mode shapes. Shown in Fig. 3 are the first seven mode shapes and natural frequencies of an eight-turn OHP (Fig. 1(a)). Water is charged into the capillary tube with a charging ratio r_c = 60% (see Fig. 10(e)) and the OHP consists of 48 liquid slugs separated by 48 vapor slugs. The lengths and positions of liquid and vapor slugs are assumed using a normal random distribution function. Due to nonlinearities of vapor slugs, the spring constant of each vapor slug changes with its temperature and displacements of its neighboring fluid slugs. The linear modal analysis here is performed using the initial setup conditions. Because the OHP is looped, the liquid slugs can circulate in the capillary tube without restraint. This free-restraint problem is not commonly seen in the analysis of mechanical systems, and it results in the chaotic performance of the slug flow.

Fig. 3(a) shows the first oscillation mode of the OHP. The 48 red[1] points represent the 48 liquid slugs, and the same displacement for all liquid slugs indicates that they move along the same direction with zero phase difference between fluid slugs. In other words, it is a circulation flow, and it is also called the rigid-body mode for a mechanical system. Because the natural frequency of the first mode is zero, the circulation flow is also called the zero-frequency mode. This circulation of liquid slugs moves the high-temperature, high-pressure vapor slugs to the condenser. If the circulation is stopped,

[1] For interpretation of color in Figs. 3 and 4, the reader is referred to the web version of this article.

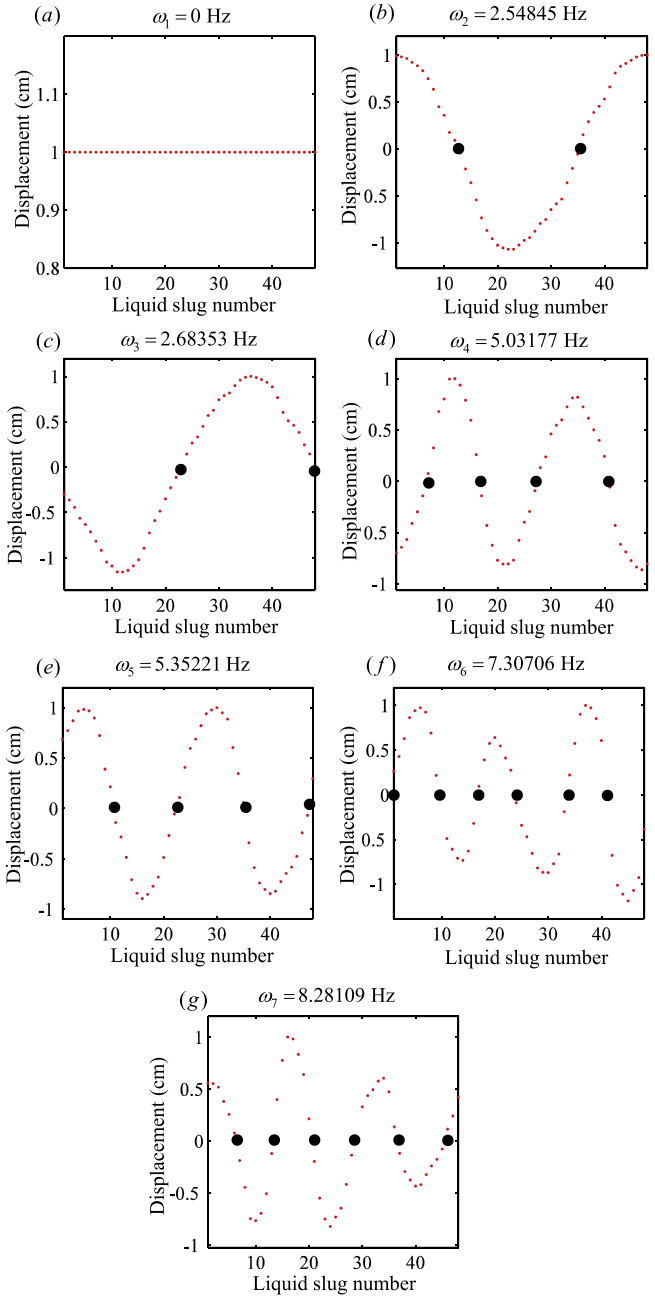

Fig. 3. Modal oscillations of liquid slugs within the OHP: (a) 1st mode, (b,c) 2nd & 3rd modes, (d,e) 4th & 5th modes, and (f,g) 6th & 7th modes.

vapor slugs in the condenser region will disappear and liquid slugs will be pushed to the condenser region. That is an important failure mode for an OHP.

Fig. 3(b) and (c) show the second and third modes and their natural frequencies. Both have two vibration nodes (black dots) and almost the same frequency. They exist because the OHP configuration is symmetric. The small discrepancy between the two natural frequencies is caused by the random and asymmetric distribution of liquid slugs. When the liquid slugs harmonically oscillate at the second (or third) natural frequency, liquid slugs around the two vibration nodes are almost stagnant. Similar to the second and third modes, modes having four and six vibration nodes also exist in pair and have almost the same frequency. Fig. 3(d) and (e) show the pair of vibration modes with four nodes, and Fig. 3(f) and (g) show the pair of vibration modes with six nodes. The actual oscillation amplitude of a high-frequency mode is often small because the vibration energy is proportional to (amplitude × frequency)^2. In other words, the participation of high-frequency modes in an ordinary linear mechanical system is often minor. For a nonlinear system, however, the participation of high-frequency modes may play an important role in system dynamics and stability [34–36]. For a real multi-turn OHP, the zero-frequency mode is crucial to its performance. How to initiate an OHP is mainly answered by how to generate and maintain its zero-frequency mode. Although the high-frequency modes do not contribute much to the circulation, the liquid slugs' high-frequency and high-velocity oscillations create high temperature gradients to increase the heat transfer between the liquid slugs and the tube wall. Following this line of thinking, one can imagine that an appropriate combination of different modal vibrations by design or control can result in an OHP with high heat transfer capability. Next we consider the influences of different factors on the performance of an OHP. For the purpose of comparison, we present the performance of an OHP filled with ammonia as the reference case.

7.2. Referential case: OHP with ammonia as the working fluid

Because ammonia has a small dynamic viscosity, a high thermal conductivity and a low latent heat, it is usually chosen as the working fluid for a multi-turn OHP. In order to investigate the influential factors for design of OHPs, a referential case with ammonia is presented first. The parameters of the eight-turn referential OHP are shown in Table 1 and L_e, L_c and L_a represent length of evaporator, condenser and adiabatic section, respectively.

Because the liquid slug motions tend to be chaotic when heat is added to the evaporator region, the initial velocities of liquid slugs are assumed by using a Gaussian (or normal) distribution function. The Gaussian distribution $\mathcal{N}(1,2^2)$ shown in Table 1 means the velocities of all liquid slugs have a mean value of 1.0 m/s and a standard deviation of 2.0 m/s. The mean velocity indicates the tendency of all liquid slugs flowing along the positive s direction shown in Fig. 1(a) and the standard deviation describes the degree of chaotic motion. The OHP is placed along the vertical direction and heat is added to the bottom part. The vapor slugs expand in the evaporator and contract in the condenser, which causes the random oscillation of the liquid slugs. The liquid slugs start to circulate when the average velocity of the liquid slugs is big enough. The vapor and liquid slugs have the same initial temperature at 55 °C. In real experiments, the condenser temperature is often known and constant, and the evaporator temperature is often unknown but the input heat flux is known. In the simulations here, however, the condenser temperature is fixed at 40 °C, and the evaporator temperature is also fixed at a constant temperature 80 °C in order to simplify the solution process and accelerate the simulation. The phase-change heat transfer coefficients between vapor slugs and the tube wall needed for Eq. (12) can be estimated

Table 1
Parameters of the referential OHP.

Dimensions of the OHP	L_e:L_a :L_c = 3:1:3 L_e = L_c = 9.64 cm, L_a = 3.21 cm
Orientation	Vertical
Distribution of initial velocities	$\mathcal{N}(1,2^2)$ (m/s)
Initial vapor and liquid temperature	55°C
Heating mode	Bottom heating
Temperature of the evaporator	80 °C
Temperature of the condenser	40 °C
Working fluid	Ammonia
Charging ratio	r_c = 60%
Bending pressure loss coefficient	C_b = 0%
Tube diameter	D = 4 mm

using Eq. (31). Twenty non-uniform elements are used for each liquid slug in the finite element model and a laptop with i5 CPU @2.67 GHz and 6G RAM is utilized for computation. The average computational time needed for each case of 16-s numerical simulation is about 2 wall-clock hours.

Fig. 4(a) shows how the velocity of the first liquid slug varies within the first 16 s. The velocity changes at a high frequency within the first 0.5 s because high-frequency interactions between liquid slugs happen at the beginning due to random distribution of initial velocities. In the steady state, the circulation of the slug flow sustains with a mean velocity of about 1.2 m/s. Meanwhile, the velocity of the first liquid slug oscillates at a low frequency from $t = 2$ s to $t = 16$ s in Fig. 4(a). When a liquid slug moves from the evaporator section to the condenser section, the pressure difference overcomes the gravitational and frictional forces, and the liquid slug accelerates until it passes the turn on the condenser side. Then the liquid slug moves from the low pressure area (i.e., the condenser) to the high pressure area (i.e., the evaporator) and the velocity of the liquid slug decreases. The low-frequency variation of the liquid slug's velocity is due to changes of the moving direction, i.e., from the evaporator (or condenser) to the condenser (or evaporator). When the slug flow circulates at a higher velocity, the variation frequency is also higher. The velocities from the 1st second to the 15th second in Fig. 4(a) are taken as samples for time–frequency analysis using Hilbert–Huang transform (HHT) [37]. The green line in Fig. 4(a) is the moving average of the velocity. After taking out the moving average and noise, the variation of velocity is shown in Fig. 4(b) with a blue line. The noise is eliminated from the signal using a signal conditioning technique based on the empirical mode decomposition (EMD) [37]. The black and red lines overlapped by the blue line are the velocity signal with noise. Fig. 5 shows the results of HHT analysis of the velocity signal shown in Fig. 4(b). Only one intrinsic mode function (IMF) is extracted from the original signal and the instantaneous amplitude (IA) and instantaneous frequency (IF) of the velocity are shown in Fig. 5(c) and (d). The IA and IF oscillates with respect to (w.r.t.) constant average values 0.25 m/s and 2.7 Hz, respectively. The variation of the liquid slug's velocity creates a large velocity gradient and therefore promotes the forced heat transfer between the liquid slug and the capillary tube wall.

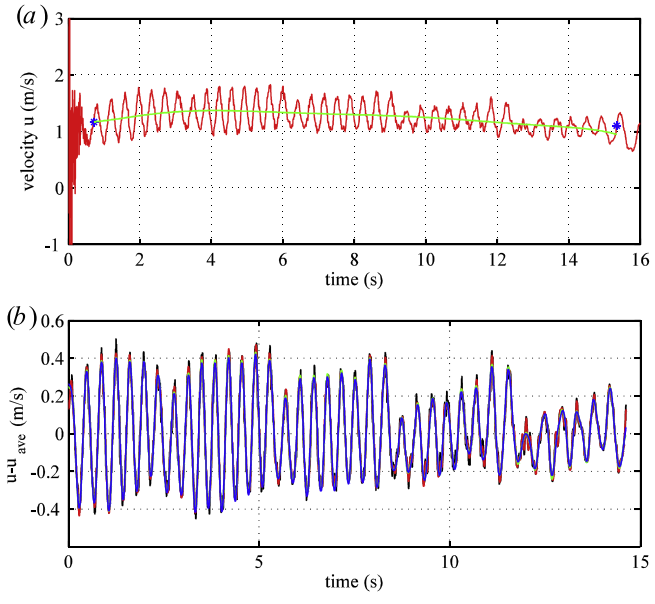

Fig. 4. The first liquid slug's velocity (referential case): (a) velocity, and (b) a data segment selected for HHT analysis. Here $u = \dot{s}_1$.

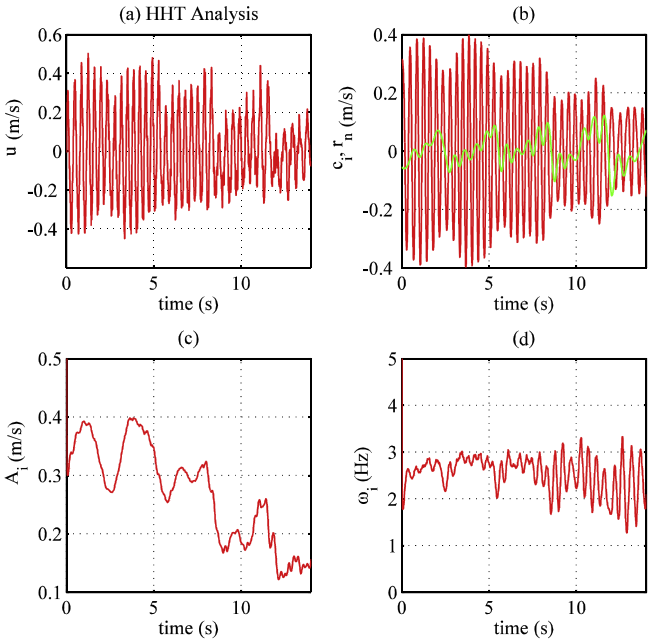

Fig. 5. HHT analysis of the first liquid slug's velocity (referential case): (a) velocity without the moving average, (b) IMFs and the residual, (c) instantaneous amplitude, and (d) instantaneous frequency.

Fig. 6 shows how the average temperature of all liquid slugs changes with time. The average temperature is calculated using the following formula

$$T_{ave} = \frac{\sum_{j=1}^{M}\sum_{i=1}^{N_{ej}} L_{ji}(T_{ji} + T_{j(i+1)})/2}{\sum_{j=1}^{M} L_j} \tag{55}$$

where M(=48) is the total number of liquid slugs, $N_{ej}$is the total number of elements within the jth liquid slug, $T_{ji}$is the temperature at the ith node of the jth liquid slug, L_{ji} is the elemental length of the ith element of the jth liquid slug, and L_j is the length of the jth liquid slug. Because the initial temperature of the vapor and liquid slugs is 55 °C, the curve begins at 55 °C and then increases to and saturates at about 59 °C. When the average temperature of the liquid slugs gets closer to the steady state temperature, the slope of the curve

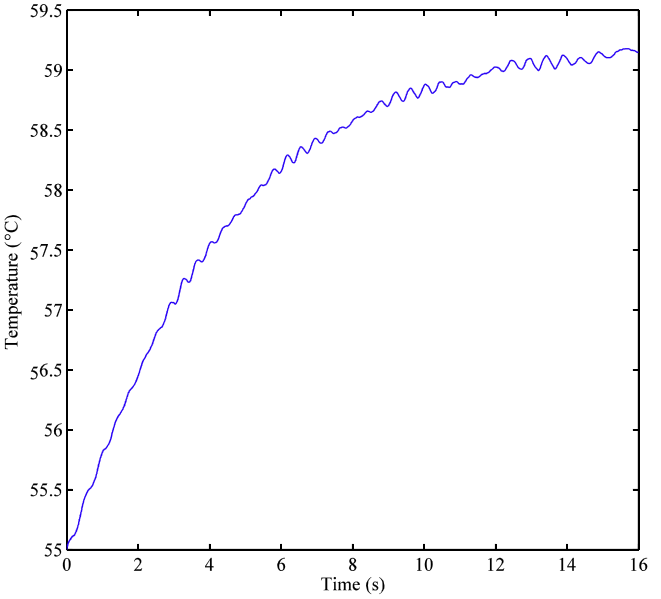

Fig. 6. The time-varying average temperature of all liquid slugs (referential case).

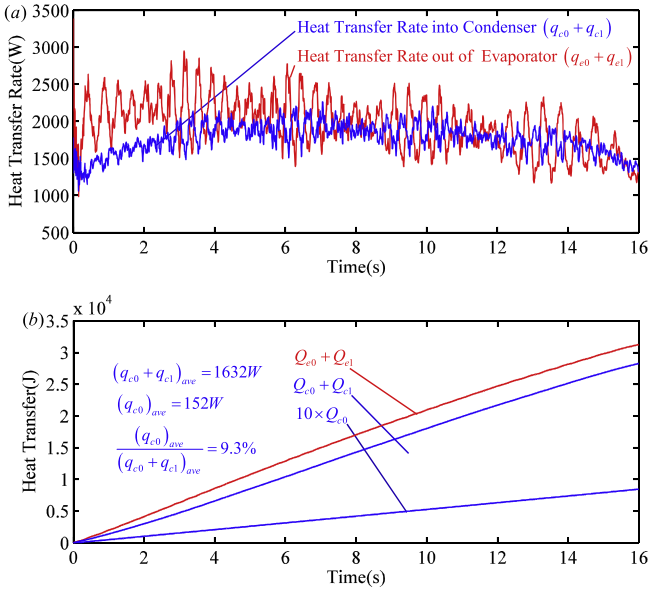

Fig. 7. Heat transfer performance (referential case): (a) heat transfer rates, and (b) total amounts of transferred heat.

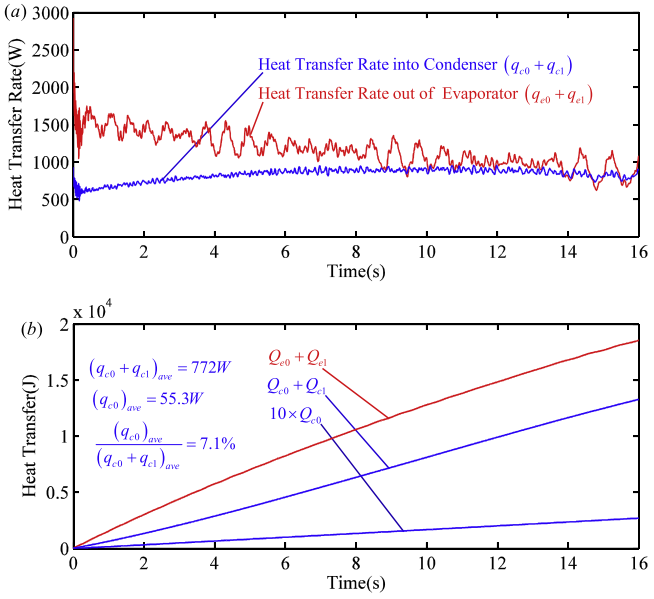

Fig. 8. Heat transfer performance (T_e = 70 °C and T_c = 50 °C): (a) heat transfer rates, and (b) total amounts of transferred heat.

becomes smaller. At the 12th second, the curve is almost flat, indicating the slug flow has reached a thermally steady state. One may note that the steady-state temperature (59.2 °C) is slightly lower than the average of the evaporator and condenser temperatures (60 °C). This is because the condenser-tube contact area is slightly larger than the evaporator-tube contact area due to the top horizontal segment, as shown in Fig. 1(a).

Fig. 7 shows the heat transfer rates and total amounts of heat transferred into the condenser and out of the evaporator. Results show that the heat transfer efficiency between the liquid slugs and the capillary tube depends on three factors: (1) the contact areas between the liquid slugs and the condenser and evaporator, (2) the temperature differences between the liquid slugs and the condenser and evaporator, and (3) the effective heat transfer coefficient between the liquid slugs and the tube wall. Because the temperature of liquid slugs at the initial state is relatively low compared with their steady state temperature, the heat transfer rate out of the evaporator is higher than the heat transfer rate into the condenser. During this period, the average temperature increases as shown in Fig. 6. After the 8th second, the heat transfer rate into the condenser region, q_c, and that out of the evaporator region, q_e, almost balance with each other. The heat transfer rates q_c and q_e decrease from the 8th second to the 16th second because the slug-flow velocity decreases as shown in Fig. 4(a). Fig. 7(b) shows the accumulated amounts of heat transferred out of the evaporator and into the condenser, denoted by $Q_{e0}+Q_{e1}$ and $Q_{c0}+Q_{c1}$, respectively. The amounts of heat transfer out of the condensation and into the evaporation through vapor slugs are denoted by $Q_{c0}$and Q_{e0}. A steady-state average heat transfer rate into the condenser region is estimated using the total amount of heat transferred between the 14th second and the 16th second. The average steady-state heat transfer rate of the OHP is calculated to be 1632 W, of which the latent heat transfer rate is 152 W (9.3% of the total heat transfer rate). This proves that the latent heat transfer provides the driving force for the liquid-slug oscillation but the high heat transfer capability of the OHP is mainly due to the sensible heat transfer.

7.3. Influence of OHP parameters

One excellent feature of an OHP is that its thermal resistance decreases when the input heat to the evaporator increases. Fig. 8 shows the performance of an OHP with T_e = 70 °C and T_c = 50 °C. Other parameters of the OHP remain the same as those of the reference case shown in Table 1. The IF of the OHP is about 2 Hz and is smaller than the IF of the referential case (2.7 Hz). The steady state velocity of the first liquid slug is also lower than that of the referential case. This proves that a higher $T_e - T_c$ can generate a stronger slug flow and in turn increases the heat transfer capability of the OHP. The initial temperature of the vapor and liquid slugs is at 55 °C and it takes about 16 s to reach its steady-state temperature 59.2 °C. Because the temperature difference $T_e - T_c$ is smaller than the referential case, it takes longer time for the liquid slugs to reach the thermally steady state. The heat transfer rate out of the evaporator is much higher than that into the condenser because the liquid slugs stay in low temperature for a long time. The average heat transfer rate of the OHP is 772 W. The heat transfer capability of the OHP drops by 53% when $T_e - T_c$ drops from 40 °C to 20 °C.

Table 2
Physical properties of different working fluids.

Working fluids	Density kg/m^3	Dynamic viscosity N · s/m^2	Latent Heat kJ/kg	Specific heat kJ/(kg · K)	Thermal conductivity W/(m · K)	Surface tension mN/m	Outstanding features
Water	983.28	4.63×10^{-4}	2308.9	4.1847	0.6527	66.1	high latent heat
Acetone	744	2.26×10^{-4}	495	2.2959	0.1689	18.7	low latent heat
Ammonia	545.7	9.88×10^{-5}	872.95	5.1414	0.402	13	low viscosity

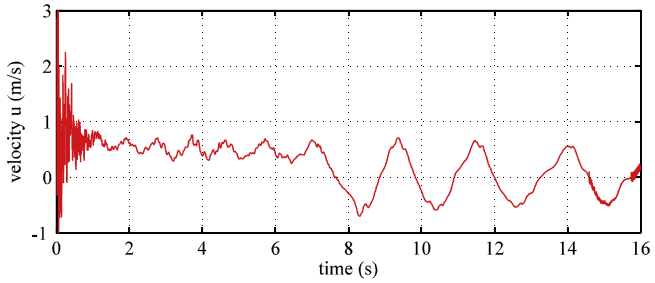

Fig. 9. The first liquid slug's velocity (water).

The latent heat transfer rate is 55.3 W and accounts for 7.1% of the total heat transfer rate.

Different working fluids such as R123, R142b, ethanol, FC-72, FC-75, water, acetone and ammonia are widely used in experiments. The physical properties of working fluids have strong influences on OHPs. Physical properties of water, acetone and ammonia are list in Table 2. Circulation is commonly observed in OHPs with ammonia and acetone as working fluids, but no circulation is easily formed in OHPs with water [5]. One possible explanation is the high viscosity of water. Fig. 9 shows that, when water is used in an OHP, the liquid slugs start to circulate with a low velocity between $t = 1$ s but the circulation stops at $t = 7$ s. After $t = 7$ s, only local oscillation within each turn can be observed. The IF and IA of the first liquid slug's velocity in an acetone OHP are about 1.8 Hz and 0.2 m/s, which are much higher than the 1 Hz and 0.1 m/s in the water OHP. The low latent heat of acetone contributes to the strong oscillation of the liquid slugs. The average heat transfer rate of the acetone OHP at the steady state is 853 W of which the latent heat transfer rate is 125 W (14.7% of the total heat transfer rate). The acetone OHP's strong motion of liquid slugs but a relatively low heat transfer capability can be explained by its low

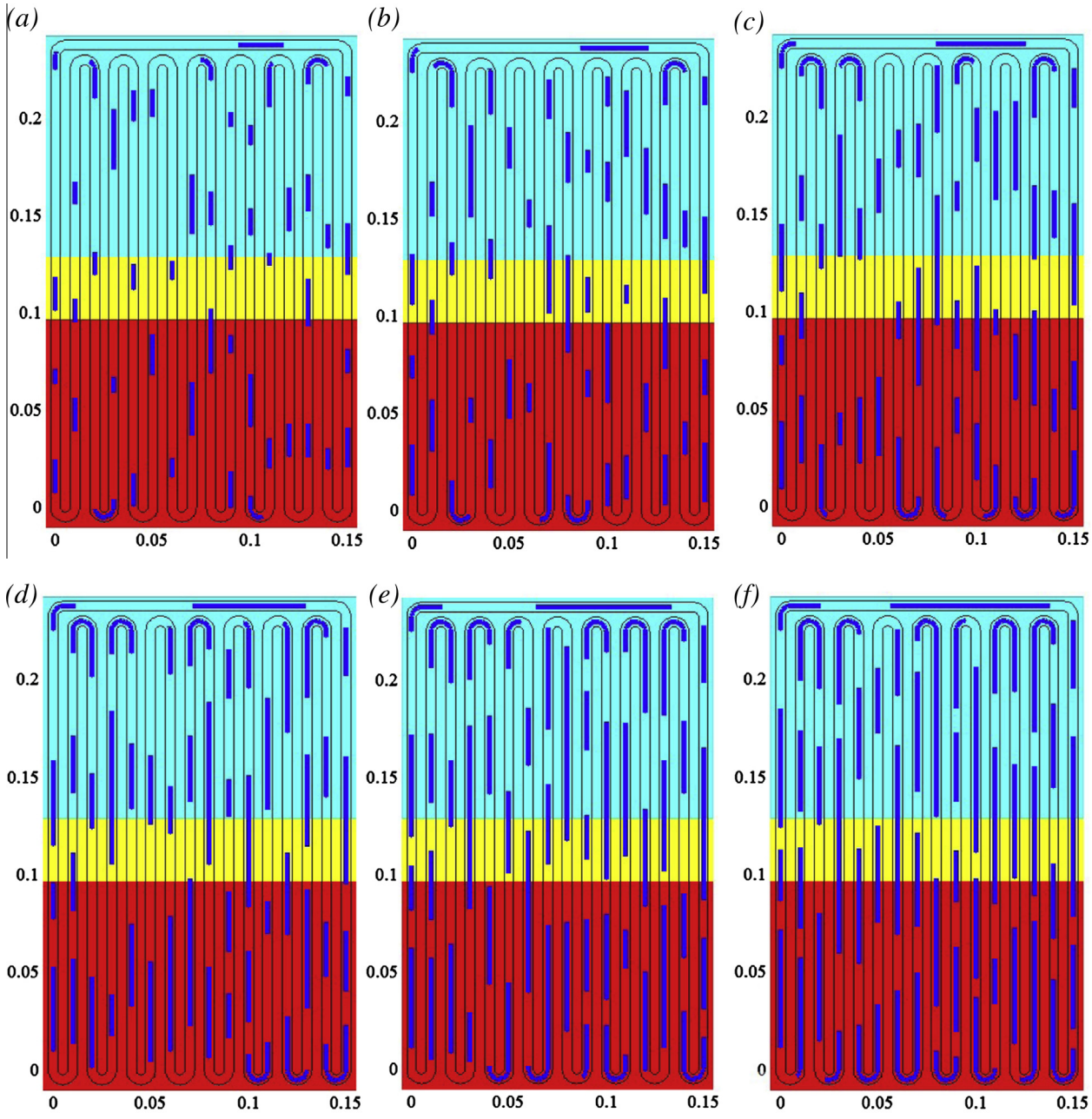

Fig. 10. OHPs with different charging ratios r_c: (a) 20%, (b) 30%, (c) 40%, (d) 50%, (e) 60%, and (f) 70%.

Table 3
Performance of OHPs with different charging ratios.

Charging ratios (%)	Average IAs (m/s)	Average IFs (Hz)	Time needed to reach steady state (s)	Average heat transfer rate (W)	Average latent heat transfer rate (W)	Percentage of latent heat (%)
20	0.29	3.2	9	733	122	16.6
30	0.25	2.5	11	917	128.4	14
40	0.25	2.4	12	1185	145.8	12.3
50	0.25	2.3	12	1422	151	10.6
60	0.25	2.7	12	1632	152	9.3
70	0.16	2	16	984	55.1	5.6

Table 4
Performance of OHPs with different bending-pressure-loss coefficients.

Bending pressure loss coefficients	Average IAs (m/s)	Average IFs (Hz)	Time needed to reach steady state (s)	Average heat transfer rate (W)	Average latent heat transfer rate (W)	Percentage of latent heat (%)
0	0.25	2.7	12	1632	152	9.3
0.2	0.25	1.7	16	1327	96.9	7.3
0.5	0.2	1.7	16	966	62	6.4

thermal conductivity. The thermal conductivity of acetone is only 0.1689 W/(m · K) at 60 °C, which is 42% of ammonia and 25.9% of water under the same temperature.

Fig. 10 illustrates six OHPs with different charging ratios ranging from 20% to 70%. Other parameters of these OHPs remain the same as those of the reference case shown in Table 1. Table 3 summarizes the performance of the 6 OHPs. In general, when the charging ratio r_c increases, the driving force decreases but the heat transfer capability increases. This is because the contact area between the liquid slugs and the tube wall increases when r_c increases. However, when the charging ratio increases up to 70%, heat transfer capability of the OHP decreases due to lack of driving force. It can be concluded that the optimum charging ratio is between 50% and 60%. With a low charging ratio, the IA, IF and latent heat transfer of the OHP are high because the contact area between the vapor slugs and the tube wall is large. The time needed to reach the steady state is short because the mass inertia of the liquid slugs is low with a low charging ratio. The heat transfer rate into the condenser, q_c, and that out of the evaporator, q_e, increase with the oscillation amplitude when the charging ratio decreases. This is because the strong oscillation of the liquid slugs increases the heat transfer rates between the liquid slugs and the tube wall and the contact areas between the liquid slugs and the evaporator and condenser.

The pressure loss at the bending area slows down the liquid slugs' motion and hence reduces the heat transfer capability of an OHP. Table 4 summarizes and compares the performances of OHPs with different values for the bending pressure loss coefficient C_b. When C_b increases from 0 to 0.5, the average IA and IF decrease from 0.25 m/s to 0.2 m/s and from 2.7 Hz to 1.7 Hz, and the heat transfer rate decreases by 666 W, respectively. This is because the motion of liquid slugs is prohibited when liquid slugs pass the bending area. When the number of turns in the OHP increases and the turn radius a (see Fig. 1(a)) of the turns decreases, the pressure loss becomes more significant. In order to reduce the pressure loss at bends, small curvatures at bending areas are desired.

Top-heating and bottom-heating modes are commonly used heating modes for OHPs. The difference between these two modes is the gravity direction and hence influence of gravity is discussed together with the influence of heating modes here. Other parameters of the OHP remain the same as those of the referential case. For a horizontally oriented OHP, the liquid slugs begin to circulate and oscillate under the initial conditions because an initial velocity field *cal* $N(1,2^2\text{m/s})$ is assigned to the fluid slugs. But the velocities of the liquid slugs decrease very quickly and some liquid slugs start to have difficulty in moving from the condenser section to the evaporator section. Fig. 11(a) shows the potential energy variation of a liquid slug in a horizontal OHP. The horizontal axis represents the curvilinear coordinate s of the looped OHP and the vertical axis represents the potential energy. Because the vapor pressure in the evaporator is higher than the vapor pressure in the condenser, a liquid slug has a higher potential energy in the evaporator region and a lower potential energy in the condenser region. The first turn is assumed to be in the evaporator region (see Fig. 1(a)) and the potential energy of a liquid slug changes periodically because the

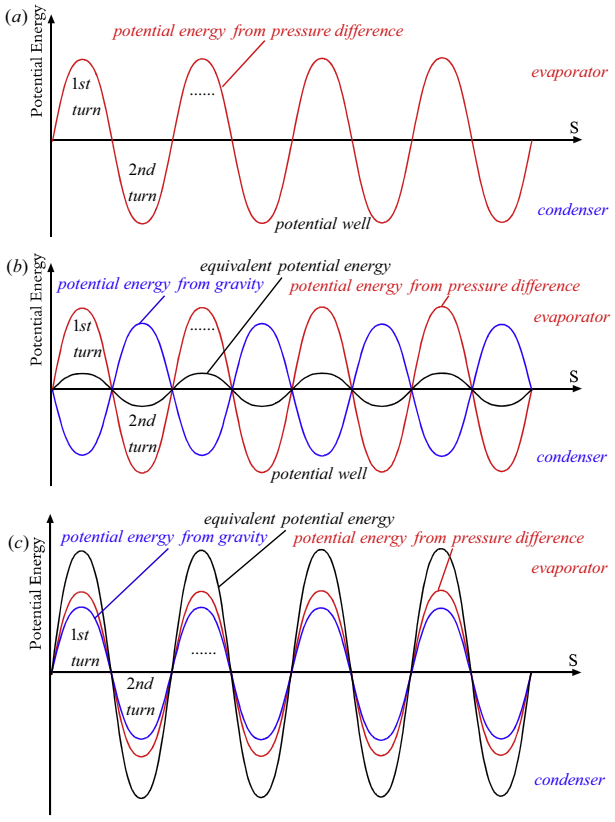

Fig. 11. Potential energy analysis: (a) horizontal OHP, (b) referential, vertical bottom-heating OHP, and (c) vertical top-heating OHP.

potential energy at the turns in the condenser region has minimum values. This explains why the liquid slugs are usually pushed to the condenser side at the beginning. When an OHP is horizontally oriented, the potential well produced by the pressure difference between the evaporator and condenser is large enough to entrap the liquid slug and only local oscillation at the condenser side can be observed. When the OHP is vertically oriented, the gravity field also produces potential energy for each liquid slug. If the OHP is heated from the bottom part, the phase relationship between the potential energy from gravity and that from pressure difference can be described in Fig. 11(b). The potential wells of the total potential energy are small and hence the vertical OHP with bottom-heating mode works. Fig. 11(c) shows the potential energy of the vertical OHP with top heating. When a liquid slug moves from the condenser to the evaporator, the potential energy from gravity and the potential energy from the pressure difference increase at the same time. The liquid slugs can be easily trapped by the potential wells. However, one also needs to mind that the potential energy from pressure difference is often non-smooth and even chaotic because of the random sizes and nonlinear oscillations of vapor slugs.

8. Concluding remarks

Presented here is an advanced, fully nonlinear thermomechanical finite-element model of multi-turn oscillating heat pipes that can accurately simulate the fluid slug oscillation and calculate the time-varying spatial distributions of temperature of fluid and vapor slugs and the global heat transfer efficiency of an oscillating heat pipe. The influences of nonlinear spring effect of vapor slugs, mass transferring effect, fluid filling ratio, operating temperature, gravity, bending pressure loss, temperature difference between the evaporator and condenser, properties of the working fluid, and different random distributions of initial velocities and lengths of fluid slugs on the heat transfer of OHPs are studied in detail. Results show that an OHP is a parametrically excited nonlinear thermomechanical system with the latent heat transfer as the driving force and the oscillation-induced sensible heat transfer as the main heat transfer mechanism. The oscillation frequency is mainly determined by the fluid plug mass and the ratio of the vapor plug length and the pipe's cross-sectional area. The proposed thermomechanical model can be used for detailed and accurate simulations of dynamics and heat transfer of OHPs and hence can be used for their design optimization.

Acknowledgment

This work is supported by the Office of Naval Research under Grant N000114-11-1-0334. The support is gratefully acknowledged.

References

[1] G. Karimi, J.R. Culham, Review and assessment of pulsating heat pipe mechanism for high heat flux electronic cooling, in: ITHERM '04. The Ninth Intersociety Conference on, Thermal and thermomechanical phenomena in electronic systems, 2004, pp. 52–59.
[2] H.B. Ma, B. Borgmeyer, P. Cheng, Y. Zhang, Heat transport capability in an oscillating heat pipe, J. Heat Transfer 130 (8) (2008) 081501.
[3] L.T. Yeh, Review of heat transfer technologies in electronic equipment, J. Electron. Packag. 117 (4) (1995) 333.
[4] A.J. Jiao, H.B. Ma, J.K. Critser, Heat transport characteristics in a miniature flat heat pipe with wire core wicks, J. Heat Transfer 130 (5) (2008) 051501.
[5] Y. Zhang, A. Faghri, Advances and unsolved issues in pulsating heat pipes, Heat Transfer Eng. 29 (1) (2008) 20–44.
[6] G.P. Peterson, An Introduction to Heat Pipes: Modeling, Testing and Application, Wiley, New York, 1994.
[7] H. Yang, S. Khandekar, M. Groll, Operational limit of closed loop pulsating heat pipes, Appl. Therm. Eng. 28 (1) (2008) 49–59.
[8] W. Shao, Y. Zhang, Effects of film evaporation and condensation on oscillatory flow and heat transfer in an oscillating heat pipe, J. Heat Transfer 133 (4) (2011) 042901.
[9] M.B. Shafii, A. Faghri, Y. Zhang, Thermal modeling of unlooped and looped pulsating heat pipes, J. Heat Transfer 123 (6) (2001) 1159.
[10] A. Jiao, H. Ma, J. Critser, Experimental investigation of cryogenic oscillating heat pipes, Int. J. Heat Mass Transfer 52 (15–16) (2009) 3504–3509.
[11] J. Xu, Y. Zhang, H. Ma, Effect of internal wick structure on liquid-vapor oscillatory flow and heat transfer in an oscillating heat pipe, J. Heat Transfer 131 (12) (2009) 121012.
[12] P. Cheng, H.B. Ma, Mathematical model of an oscillating heat pipe, Int. J. Heat Transfer Eng. 32 (11) (2011) 1037–1046.
[13] S.M. Thompson, H.B. Ma, R.A. Winholtz, C. Wilson, Experimental investigation of miniature three-dimensional flat-plate oscillating heat pipe, J. Heat Transfer 131 (4) (2009) 043210.
[14] I. Yoon, Two-phase flow dynamics by real-time neutron imaging in oscillating heat pipe, University of Missouri, Columbia, University of Missouri, Columbia, 2008.
[15] H. Akachi, F. Polasek, P. Stulc, Pulsating heat pipes, in: Heat Pipe Technology: Theory, Applications and Prospects (International Heat Pipe Conference Proceedings), Melbourne, Australia, 1996.
[16] S. Khandekar, M. Schneider, P. Schafer, R. Kulenovic, M. Groll, Thermofluid dynamic study of flat plate closed loop pulsating heat pipe, Microscale Thermophys. Eng. 6 (4) (2002) 303–318.
[17] S. Khandekar, N. Dollinger, M. Groll, Understanding operational regimes of pulsating heat pipes an experimental study, Appl. Therm. Eng. 23 (6) (2003) 707–719.
[18] S. Maezawa, R. Nakajima, K. Gi, H. Akachi, Experimental study on chaotic behavior of thermohydraulic oscillation on oscillating thermosyphon, in: Proc. Fifth Int. Heat Pipe Symp., Melbourne, Australia, 1996, pp. 131–137.
[19] L. Lin, R. Ponnappan, J. Leland, Heat transfer characteristics of an oscillating heat pipe, in: Proc. 34th AIAA Thermophysics Conf., Denver, Colorado, 2000, pp. 2000–2218.
[20] Y. Miyazaki, H. Akachi, Heat transfer characteristics of looped capillary heat pipe, in: Proceedings of the Fifth Int. Heat Pipe Symp., Melbourne, Australia, 1996, pp. 378–383.
[21] V.M. Kiseev, K.A. Zolkin, The influence of acceleration on the performance of oscillating heat pipe, in: Proc. 11th Int. Heat Pipe Conf., Tokyo, Japan, 1999, pp. 154–158.
[22] Y. Miyazaki, H. Akachi, Self-excited oscillation of slug flow in a micro channel, in: Proc. Third Int. Conf. Multiphase Flow, Lyon, France, 1998.
[23] M. Hosoda, S. Nishio, R. Shirakashi, Meandering closed loop heat transport tube (propagation phenomena of vapor plug), in: Proc. Fifth ASME/JSME Joint Thermal Engineering Conf., San Diego, California, 1999.
[24] Y. Zhang, A. Faghri, Heat transfer in a pulsating heat pipe with open end, Int. J. Heat Mass Transfer 45 (4) (2002) 755–764.
[25] Y. Zhang, A. Faghri, M.B. Shafii, Analysis of liquid–vapor pulsating flow in a U-shaped miniature tube, Int. J. Heat Mass Transfer 45 (12) (2002) 2501–2508.
[26] Y. Zhang, A. Faghri, Oscillatory flow in pulsating heat pipes with arbitrary numbers of turns, J. Thermophys. Heat Transfer 17 (3) (2003) 340–347.
[27] K. Diethelm, N.J. Ford, A.D. Freed, A predictor-corrector approach for the numerical solution of fractrional differential equations, Nonlinear Dyn. 29 (1–4) (2002) 3–22.
[28] J.C. Chen, Correction for boiling heat transfer to saturated fluids in convective flow, Ind. Eng. Chem. Process Des. Dev. 5 (3) (1966) 8.
[29] W. Shao, Y. Zhang, Thermally-induced oscillatory flow and heat transfer in an oscillating heat pipe, J. Enhanced Heat Transfer 18 (3) (2011) 177–190.
[30] R.W. Schrage, A Theoretical Study of Interphase Mass Transfer, Columbia University Press, 1953.
[31] P. Davidovits, D.R. Worsnop, J.T. Jayne, C.E. Kolb, P. Winkler, A. Vrtala, P.E. Wagner, M. Kulmala, K.E.J. Lehtinen, T. Vesala, M. Mozurkewich, Mass accommodation coefficient of water vapor on liquid water, Geophys. Res. Lett. 31 (22) (2004) 4.
[32] J. Voigtländer, F. Stratmann, D. Niedermeier, H. Wex, A. Kiselev, Mass accommodation coefficient of water: a combined computational fluid dynamics and experimental data analysis, J. Geophys. Res. 112 (D20) (2007).
[33] V.P. Carey, Liquid-Vapor Phase-Change Phenomena: An Introduction to The Thermophysics of Vaporization and Condensation Processes in Heat Transfer Equipment, Hemisphere Publishing Corporation, 1992.
[34] P.F. Pai, Highly flexible structures: modeling, computation, and experimentation, American Institute of Aeronautics and Astronautics, 2007.
[35] A.H. Nayfeh, D.T. Mook, Nonlinear Oscillations, Wiley, 1995.
[36] F.C. Moon, Chaotic Vibrations: An Introduction For Applied Scientists And Engineers, Wiley, 1987.
[37] P.F. Pai, Time–frequency characterization of nonlinear normal modes and challenges in nonlinearity identification of dynamical systems, Mech. Syst. Signal Process. 25 (7) (2011) 2358–2374.